ACS SENSORS

pubs.acs.org/acssensors

Letter

A Multiplexable Plasmonic Hairpin-DNA Sensor Based On Target-specific Tether Dynamics

Jeanne Elisabeth van Dongen,* Laurens Rudi Spoelstra, Johanna Theodora Wilhelmina Berendsen, Joshua Taylor Loessberg-Zahl, Jan Cornelis Titus Eijkel, and Loes Irene Segerink

Cite This: *ACS Sens.* 2021, 6, 4297–4303

Read Online

ACCESS | Metrics & More | Article Recommendations | Supporting Information

ABSTRACT: The need for measurements of multiple biomarkers simultaneously at subnanomolar concentrations asks for the development of new sensors with high sensitivity, specificity, precision, and accuracy. Currently, multiplexed sensing in single molecule sensors increases the complexity of the system in terms of reagents and sample read-out. In this letter, we propose a novel approach to multiplex hairpin-based single-DNA molecule sensors, which overcomes the limitations of the present approaches for multiplexing. By target-dependent ssDNA hairpin design, we can create DNA tethers that have distinct tether dynamics upon target binding. Our numerical model shows that by changing the stem length of the ssDNA hairpin, significantly different dynamic tether behavior will be observed. By exploiting the distance-dependent coupling of AuNPs to gold films, we can probe this dynamic behavior along the *z*-axis using a simple laser equipped microscope.

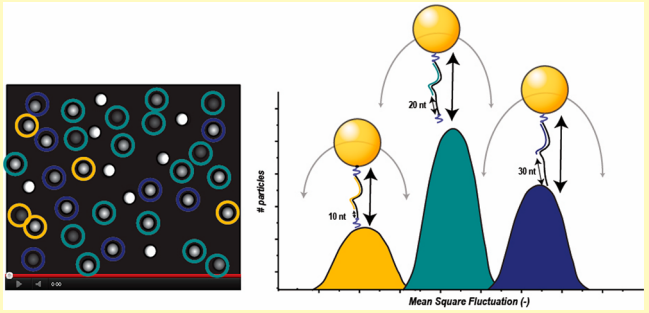

KEYWORDS: *multiplexing, biosensors, single-molecule sensing, nanoplasmonics, tethered-particle motion*

With improvements in understanding of diseases and their development, healthcare is increasingly interested in early and simultaneous detection of multiple biomarkers.[1] Multiplexing, the analysis of various biomarkers for a single disease type, has shown improvement in both sensitivity and selectivity when detecting cancer and infectious diseases.[2−4] Disease-specific biomarkers can be collected more easily than ever by using noninvasive techniques from the upcoming field of liquid biopsies. However, the typically low concentration (<nM) of these biomarkers challenges the multiplexable analytical techniques currently available in clinical chemistry, increasing the need for novel detection techniques.

Research is pushing toward biosensors with single-molecule resolution because these offer enhanced sensitivity, specificity, precision, and accuracy compared to bulk measurement techniques.[5−8] Initial near-field approaches for single molecule sensors could only detect a maximum of tens of single molecules simultaneously, which results in low-throughput detection and a limited concentration window.[9] More recently, massive parallelization of these sensors in combination with wide-field observation has allowed for measurements of hundreds if not millions of single detection events of a specific analyte, improving both detection limit and sample throughput.[5]

One downside of these wide-field single molecule techniques is their typical digital readout (they detect only target presence or absence), which does not allow differentiation between different bound targets. Therefore, multiplexing of wide-field single molecule sensors has required one of several severe increases in complexity, such as spatial separation of binding sites for different biomarkers,[10,11] washing with multiple reagents,[12] and using targets of dramatically different affinity[13] or multichannel (fluorescence) read-out.[14] These complications reduce the application of multiplexed sensors in the medical world where there is a need for reliable and simple assays. In this letter, we propose a novel approach to overcome the current limitations of multiplexed single molecule sensors. Specifically, we propose that DNA hairpin-sensors, similar to those described in literature,[15−21] besides its excellent performance in complex media,[22] may also be easily multiplexed by designing target-specific changes into the hairpins' structure. Analysis of sensor dynamics then allows easy determination of which specific sensing element has been activated.

The proposed sensor (Figure 1) will consist of thousands of individual sensing elements, each composed of a single ssDNA hairpin that tethers one gold nanoparticle (AuNP) to a gold

Received: October 1, 2021
Accepted: November 30, 2021
Published: December 1, 2021

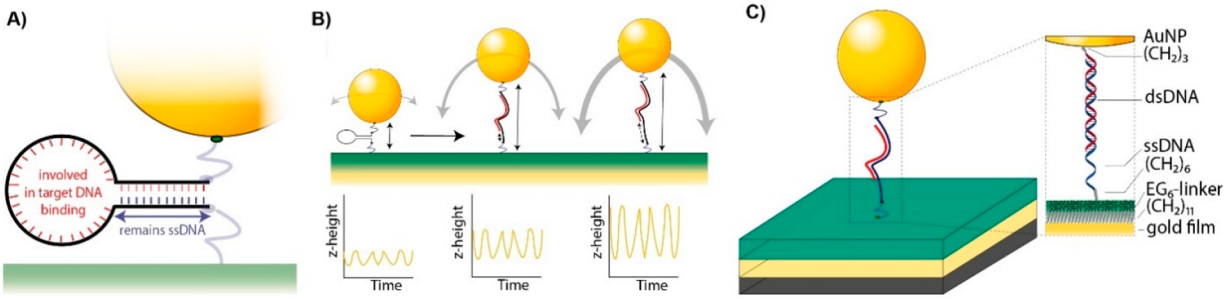

Figure 1. Schematic representation of multiplexed TPM-based sensing. (A) ssDNA molecule bound to the gold film and AuNP. Because of a self-complementary part, a stem structure will be formed that results in a so-called hairpin. Upon target binding, part of the self-complementary DNA nucleotides will bind to the target (in red), unzipping the hairpin, and resulting in a ssDNA (in blue) tether followed by a dsDNA tether. (B) Schematic representation of a sensing element prior to and after target-binding with different ssDNA lengths. The changes in the *z*-axis over time increase after target binding and are dependent on the length of original ssDNA stem, which adds to the total tether length. (C) Detailed schematic overview of a single sensing element bound to a target DNA sequence.

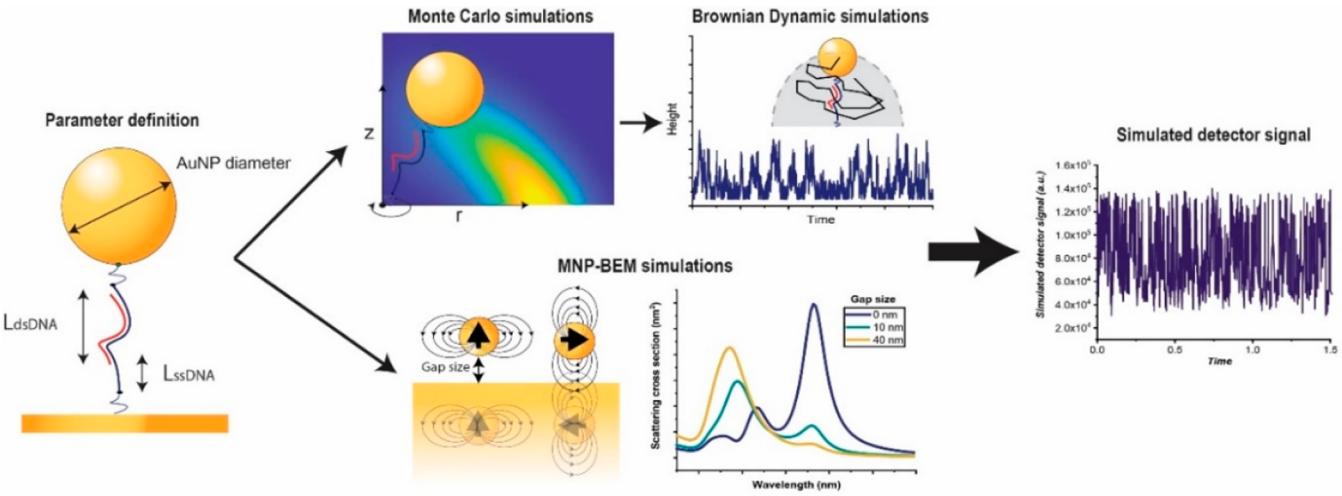

Figure 2. Schematic of the developed model consisting of the Monte Carlo simulations, Brownian dynamics simulations, and MNP-BEM simulations, that together result in the simulated detector signal.

film (Figure 1A). Upon target binding, the hairpin unfolds, changing not only the volume accessible to the AuNP but also the physical properties of the tether. Just like the typical DNA hairpin sensors described in literature,[15−20] our sensor consists of both ssDNA (originating from the self-complementary part of the hairpin-stem not involved in target binding), and double-stranded DNA (dsDNA) (Figure 1A) upon target binding. However, novelty comes from the multiplexability of our proposed sensor: by making the length of both ssDNA and dsDNA target dependent, we induce target-specific differences in both the physical properties of the tether and the volume accessible to the AuNP. These differences will be probed by looking at the dynamic behavior of the AuNP.

Our derivation of tether properties from the observed dynamics is based on the fundamentals of tethered particle motion (TPM). TPM describes the motion of microparticles connected to a substrate by a tether.[23] The tether, in this case a DNA molecule consisting of a ssDNA and dsDNA part and several linkers, confines the bead to a certain volume of space, within which Brownian motion determines the particle position over time. Because the tether properties play an important role in the movement of the particle, TPM is typically used to study tether properties like persistence length[24] and looping kinetics.[25,26] Furthermore, TPM has been used to investigate interactions between DNA and proteins such as polymerases[27] and lac repressors,[28] as these interactions induce changes in DNA flexibility. While these studies use TPM to probe unknown properties of the tether, we propose the reverse: using TPM to discriminate between different tethers of known properties, with each distinct tether type matching a specific ssDNA target molecule. To do this, we will perform simulations of the dynamic behavior of tethers consisting of different ssDNA lengths, followed by varying lengths of dsDNA. In real experiments, we could match observed TPM dynamic behavior with the behavior obtained via calibration or the simulation experiments as presented in this letter.

Because we focus on the detection of DNA sequences in liquid biopsies, the typical DNA target fragment length is <100 base pairs (bp),[29,30] which correspond to a length of ∼30 nm. This requires a relatively short total hairpin length, which limits localization precision. In current TPM experiments, read-out precision is limited by the spatial localization precision of typical optical microscopes when resolving conformational bead changes, which is typically ∼10 nm. This results in the use of >200 bp dsDNA tethers in most TPM experiments to allow precise tracking of the movement of the bead.[31,32] Here we propose to overcome the localization issue for short tethers by using plasmonic sensing, in which the distance-dependent plasmonic coupling of AuNPs to gold films

https://doi.org/10.1021/acssensors.1c02097
ACS Sens. 2021, 6, 4297−4303

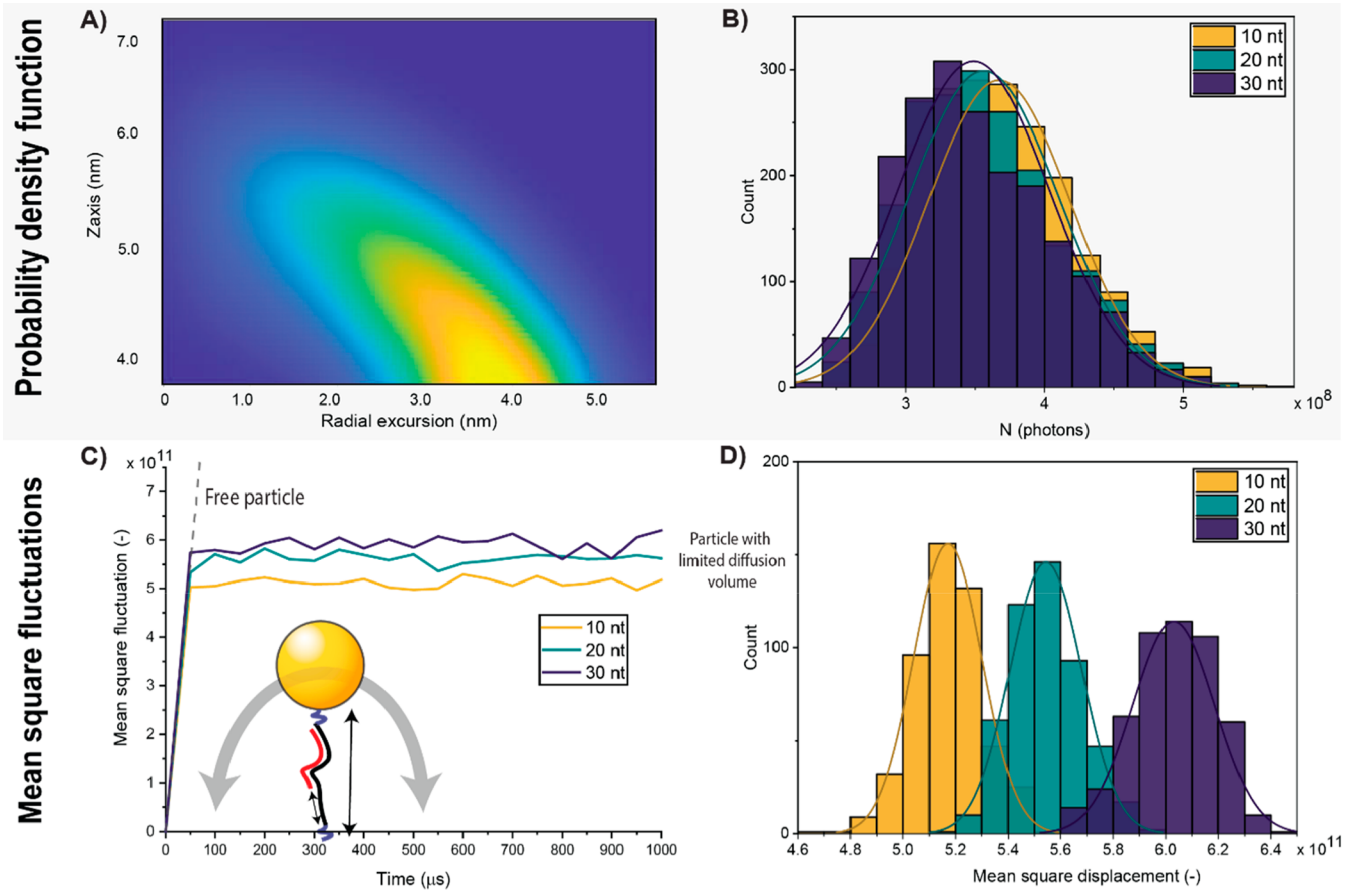

Figure 3. Comparison between average positions (A,B) and average mean square fluctuations (C,D) as discriminators for different tether properties. All results in this figure are generated for a 50 bp dsDNA strand with either a 10, 20, and 30 nt ssDNA and a simulated signal with an integration time of 50 μs. (A) Position probability map for a tether consisting of a 50 bp dsDNA strand and a 10 nt ssDNA strand. (B) Plotted distribution of the detector signal for different lengths of ssDNA. (C) Mean square fluctuation plot for increasing time step for different ssDNA strand lengths. (D) Distribution of mean square fluctuation values found for different ssDNA strand lengths..

is exploited to precisely determine particle position. Plasmonic sensing is based on the resonant scattering of a sub-100 nm AuNP, which has a resonance peak in the green region of the optical spectrum when free in a buffer.[33] When the same AuNP is placed near a gold film, the gold film acts as a mirror, and allows the AuNP to interact with its mirror image, resulting in a red-shift, comparable to the spectral shift observed for AuNP dimers.[34,35] The degree of red-shift of the AuNP scattering spectrum is strongly distance dependent, with the largest first derivative over the range of 0−50 nm, which makes this system extremely suitable to probe the changes along the *z*-axis of our tethered AuNP.[36,37]

To prove that multiplexing is indeed possible with such a sensor, we numerically predict the differences in tether composition needed to perform plasmonic multiplexed nucleotide binding assays with ssDNA hairpin tethers. A model was developed which considers both tether properties and Brownian AuNP movement in a sequential fashion, coupled to electromagnetic simulations to simulate the detected optical signal over time for different tethers (Supporting Information methods 1, 2, and 3). In short, the simulations consist of three separate steps that together form our model (Figure 2). It all starts with defining the parameters, such as the length of the ssDNA (10, 20, or 30 nucleotides (nt)) left after target binding, length of dsDNA after target binding (50−70 bp with a 2 bp step size), and AuNP size (80, 78, and 82 nm to account for polydispersity of the AuNPs used). In the first step of the model, the tether-dependent position distributions of the particles are determined using a Monte Carlo simulation method. The output of this model is a probability map of the particle positions. The second step involves the use of inverse Boltzmann statistics, where the probability distribution of the AuNP positions is converted to a potential energy map.[36,38] The potential energy map then forms the input to Brownian Dynamics simulations of the AuNP, where the potential energy results in a position-dependent force on the AuNP. From the Brownian Dynamics simulations, we obtain a time series of the AuNP position along the *z*-axis,[36,39] which then together with the plasmonic model results in the simulated detector signal. For plasmonic response calculations, electromagnetic boundary element method (BEM) simulations were performed to calculate the distance-dependent scattering and absorption of AuNPs (Supporting Information, Method 4). With the BEM simulations, the *z*-axis dependent scattering cross section of the particle can be obtained. From the positional time series obtained by the Brownian motion simulations, the probe wavelength dependent scattering cross section over time ($\sigma_{scat}(t,\lambda_{probe})$) is then calculated, which, together with setup dependent factors, results in a time-variant number of photons detected by the setup. A more elaborate explanation of the

https://doi.org/10.1021/acssensors.1c02097
ACS Sens. 2021, 6, 4297−4303

model and its considerations can be found in the Supporting Information.

Our model results in "raw" time traces, and we started with calculating the traces for an optical signal integration time of 50 μs, chosen to filter out false motion of the particle due to shot-noise or thermal expansion and/or contraction of the microscope.[25,40−43] The probability density function (PDF) of the total optical output was subsequently calculated (Figure 3A), and it was found that the average of the photon counts did not significantly differ for 50 bp DNA tethers with three different lengths of ssDNA (10, 20, 30 nt) (Figure 3B). For all other tested hairpin compositions (with varying ssDNA and dsDNA length), the same result was found (Figure S10). This indicates that the difference in possible positions introduced by different hairpin properties is averaged out by the many positions shared among the different tethered AuNPs. Differences in total photon count can thus not be used to distinguish between different tethers.

In contrast to the average photon count, the tether-dependent particle dynamics do show a significant difference between different tether lengths. The mean square fluctuation (MSF) is a measure of the deviation of the plasmonic signal with respect to a reference signal over time. It is commonly used to express the spatial extent of random motion and can be used to determine whether a particle is moving solely by diffusion or is experiencing additional forces. In this case, the additional force originates from the tether, which limits the diffusion of the AuNP compared to free diffusion, in a tether-dependent fashion (Figure 3C). We took the mean over 500 points of the maximum of the MSF curve and plotted the distribution of the values for the same tether with 50 bp dsDNA and 10, 20, and 30 nt lengths of ssDNA, as was tested in Figure 3B. The predicted MSFs in Figure 3D significantly differ ($F(10,90) = 18.681$, $p = 0.00$), demonstrating that the particles dynamics rather than average position will allow target discrimination. To study the effect of multiple tether lengths, we calculated the average MSF for DNA tethers with a size of 50−70 bp dsDNA and either 10, 20, or 30 nt of ssDNA. An (almost) linear relationship between the length of the dsDNA and the MSF can be found and the individual tether properties can clearly be distinguished (Figure 4). With a univariate analysis in SPSS followed by a post-HOC Tukey's multiple comparison test, we could determine whether the MSF of each ssDNA−dsDNA combination was significantly different from the other combinations. From this, we could conclude that a maximum of four ssDNA−dsDNA combinations could be distinguished simultaneously, which means that with the proposed sensing method four different target sequences could be measured on a single sensing surface (Supporting Information, Figure S13).

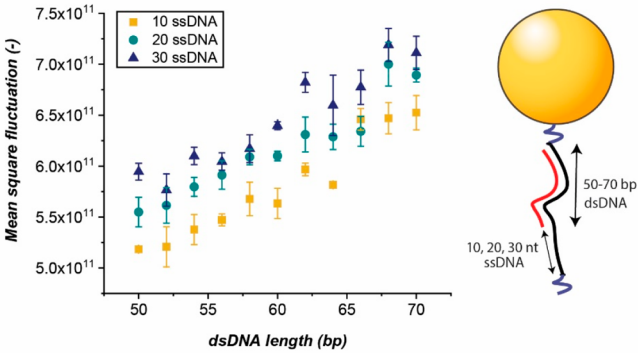

Figure 4. Mean square fluctuation of the maximum detector signal for different tether properties where $n = 3$ individual simulations for each data point. Error bars represent the mean ± sd, where $n = 3$ (three independent simulations).

The above demonstrates that a hairpin-based plasmonic sensor can be used to perform multiplexed ssDNA sensing by determining the tethered particle MSF along the z-axis. Variations in both the ssDNA length (10−30 nt) and the total tether length (60−100 nts) result in significantly different results as confirmed by ANOVA statistical testing. For 80 nm AuNPs, a single wavelength can be used to probe the z-axis MSF.

The results presented in Figure 4 do not consider some real-life measurement issues. In the next part of this letter, we will consider three main issues one could face while exploiting our sensing method and will propose practical solutions. Concerning the sensor development, it is important to know how many hairpins are needed in total to allow multiplexed sensing. The number of available AuNPs, together with the reaction kinetics of the target ssDNA with the hairpin-DNA, the target sequence concentration, the number of different targets one wants to sense, and the measurement time then determine the amount of sensing events that will be measured.[44] The lower bound for the number of sensing events will depend strongly on the analyte of interest, but with statistics we can set a minimum, based on a 10% statistical error, of 100 sensing events per analyte. For an hour of measuring at 1 nM concentration and a k_{on} of 100 μM,[45,46] this requires 2800 hairpins per target sequence. Because of the strong scattering properties of 80 nm AuNPs, a low microscope magnification is possible and up to 1000−5000 AuNPs could be followed simultaneously using a CMOS detector depending on the resolution of the detector and the needed integration time, where the point spread function of an 80 nm AuNP on average covers 870 nm^2.[47,48] Taking the new generation of affordable high speed cameras into consideration, and the integration time of around 50 μs, this means that between 300 and 1000 AuNPs can be sensed[49] Therefore, multiplexed sensing of many different target sequences requires the further development of ultrahigh resolution detectors with low magnification objectives supporting high frame rates, or a more simple solution such as moving the sensor surface along the detector to image a larger sensor surface.

For all calculations and simulations presented in this letter, we assumed AuNPs to be monodispersed with an 80 nm diameter. However, all commercially available AuNPs are polydisperse. Because we observe the variations over time of the gap size dependent plasmonic coupling of individual particles, this could cause issues when distinguishing whether changes in detector signal are due to particle or tether variations,[50,51] as the scattered intensity of a AuNP is proportional to the square of the AuNP static polarizability. Therefore, larger particles have a higher scattering intensity and a different relation between gap size and scattering intensity at a specific wavelength. We can conveniently overcome this issue by introducing a calibration step prior to target binding by imaging the hairpin-AuNPs. In Supporting Information, Method 6, we show that in the hairpin state the measured scattering intensity is mainly determined by the AuNP size as the AuNP does not have a large accessible

https://doi.org/10.1021/acssensors.1c02097
ACS Sens. 2021, 6, 4297−4303

volume. This allows easy self-calibration of the system to extract the AuNP size.

The last practical issue we would like to discuss is that short target sequences found in liquid biopsies vary considerably in size depending on the isolation method, patient, and origin of the biopsy. We therefore performed a simple check on the influence of the size of the target DNA on the dynamic fluctuations of the AuNP after target binding and found that indeed this effect was significant ($F(2,8) = 14.450$, $p = 0.005$), Supporting Information, method 7). However, if we ignore the ssDNA length and look only at total tether length (sum of ssDNA and dsDNA length = the original hairpin length), we see a significant difference between the tether lengths ($F(20,98) = 28.699$, $p = 0.000$)). Thus, if we measure ssDNA targets fragments of different lengths, we can still significantly distinguish the different tether lengths and use this for multiplexed sensing. For target lengths that exceed the length of the complementary part of the hairpin, we did not perform any simulations. Here, we anticipate two factors playing a role: long ssDNA target strands can inhibit the degrees of freedom of the AuNP relative to short DNA fragments, but as the persistence length of ssDNA is low (~2 nm (ref 52), it will be flexible and probably not significantly inhibit the movement of the particle compared to the drag force the particle is experiencing close to the surface.

In conclusion, the proposed sensing method allows robust monitoring of biomolecules with the possibility of simultaneous multiplexed gene detection with high specificity using plasmonic AuNPs that offer single-molecule read-out at a simple, laser-equipped, microscope.

■ ASSOCIATED CONTENT

Supporting Information

The Supporting Information is available free of charge at https://pubs.acs.org/doi/10.1021/acssensors.1c02097.

Elaborate explanation of the model development for the Monte Carlo simulations, Matlab implementation, Brownian dynamic simulations, Plasmonic Boundary Element Methods simulations, and effects of target sequence and AuNP size variations on the simulated data (PDF)

■ AUTHOR INFORMATION

Corresponding Author

Jeanne Elisabeth van Dongen − *BIOS Lab on a Chip Group, MESA+ & TechMed Institutes, Max Planck Center for Complex Fluid Dynamics, University of Twente, 7500 AE Enschede, The Netherlands;* orcid.org/0000-0001-9350-0394; Email: j.e.vandongen@utwente.nl

Authors

Laurens Rudi Spoelstra − *BIOS Lab on a Chip Group, MESA+ & TechMed Institutes, Max Planck Center for Complex Fluid Dynamics, University of Twente, 7500 AE Enschede, The Netherlands*

Johanna Theodora Wilhelmina Berendsen − *BIOS Lab on a Chip Group, MESA+ & TechMed Institutes, Max Planck Center for Complex Fluid Dynamics, University of Twente, 7500 AE Enschede, The Netherlands;* orcid.org/0000-0001-6464-3708

Joshua Taylor Loessberg-Zahl − *BIOS Lab on a Chip Group, MESA+ & TechMed Institutes, Max Planck Center for Complex Fluid Dynamics, University of Twente, 7500 AE Enschede, The Netherlands*

Jan Cornelis Titus Eijkel − *BIOS Lab on a Chip Group, MESA+ & TechMed Institutes, Max Planck Center for Complex Fluid Dynamics, University of Twente, 7500 AE Enschede, The Netherlands*

Loes Irene Segerink − *BIOS Lab on a Chip Group, MESA+ & TechMed Institutes, Max Planck Center for Complex Fluid Dynamics, University of Twente, 7500 AE Enschede, The Netherlands*

Complete contact information is available at: https://pubs.acs.org/10.1021/acssensors.1c02097

Author Contributions

J.E.v.D.: conceptualization, investigation, data analysis, validation, writing original draft. L.R.S.: initial code development, investigation, validation. J.T.W.B.: code development, validation, writing, reviewing, and editing. J.T.L.Z.: code development, validation, writing,reviewing, and editing. J.C.T.E.: supervising, writing, reviewing, and editing. L.I.S.: funding acquisition, supervising, writing, reviewing, and editing.

Notes

The authors declare no competing financial interest.

■ ACKNOWLEDGMENTS

We thank Emiel Visser for sharing his code for tethered particle motion simulations, which served as a starting point for the B.Sc. assignments of Lysanne Mol and Laurens Spoelstra. Lysanne Mol is acknowledged for setting up initial MNPBEM simulation during her B.Sc. project, and we thank Sergii Pud for discussions about data analysis. This project was financially supported by Stichting de Weijerhorst.

■ REFERENCES

(1) Akkilic, N.; Geschwindner, S.; Höök, F. Single-Molecule Biosensors: Recent Advances and Applications. *Biosens. Bioelectron.* **2020**, *151*, 111944.

(2) Elnifro, E. M.; Ashshi, A. M.; Cooper, R. J.; Klapper, P. E. Multiplex PCR: Optimization and Application in Diagnostic Virology. *Clinical Microbiology Reviews. Clin Microbiol Rev.* **2000**, *13*, 559−570.

(3) Brikun, I.; Nusskern, D.; Freije, D. An Expanded Biomarker Panel for the Detection of Prostate Cancer from Urine DNA. *Exp. Hematol. Oncol.* **2019**, *8* (1), 13.

(4) Bosschieter, J.; Nieuwenhuijzen, J. A.; Hentschel, A.; van Splunter, A. P.; Segerink, L. I.; Vis, A. N.; Wilting, S. M.; Lissenberg-Witte, B. I.; A van Moorselaar, R. J.; Steenbergen, R. D. A Two-Gene Methylation Signature for the Diagnosis of Bladder Cancer in Urine. *Epigenomics* **2019**, *11* (3), 337−347.

(5) Gooding, J. J.; Gaus, K. Single-Molecule Sensors:Challenges and Opportunities for QuantitativeA Nalysis. *Angew. Chem., Int. Ed.* **2016**, *55*, 11354.

(6) Manosas, M.; Camunas-Soler, J.; Croquette, V.; Ritort, F. Single Molecule High-Throughput Footprinting of Small and Large DNA Ligands. *Nat. Commun.* **2017**, *8* (1), 1−12.

(7) Taylor, A. B.; Zijlstra, P. Single-Molecule Plasmon Sensing: Current Status and Future Prospects. *ACS Sensors.* **2017**, *2*, 1103−1122.

(8) Gu, L. Q.; Shim, J. W. Single Molecule Sensing by Nanopores and Nanopore Devices. *Analyst* **2010**, *135*, 441−451.

(9) Gooding, J. J.; Gaus, K. Single-Molecule Sensors: Challenges and Opportunities for Quantitative Analysis. *Angew. Chem., Int. Ed.* **2016**, *55* (38), 11354−11366.

(10) Rissin, D. M.; Kan, C. W.; Campbell, T. G.; Howes, S. C.; Fournier, D. R.; Song, L.; Piech, T.; Patel, P. P.; Chang, L.; Rivnak, A. J.; Ferrell, E. P.; Randall, J. D.; Provuncher, G. K.; Walt, D. R.; Duffy,

D. C. Single-Molecule Enzyme-Linked Immunosorbent Assay Detects Serum Proteins at Subfemtomolar Concentrations. *Nat. Biotechnol.* **2010**, *28* (6), 595−599.
(11) Dunbar, S. A. Applications of Luminex® XMAP™ Technology for Rapid, High-Throughput Multiplexed Nucleic Acid Detection. *Clin. Chim. Acta* **2006**, *363* (1−2), 71−82.
(12) Gilboa, T.; Maley, A. M.; Ogata, A. F.; Wu, C.; Walt, D. R. Sequential Protein Capture in Multiplex Single Molecule Arrays: A Strategy for Eliminating Assay Cross-Reactivity. *Adv. Healthcare Mater.* **2021**, *10* (4), 2001111.
(13) Lubken, R. M.; de Jong, A. M.; Prins, M. W. J. Multiplexed Continuous Biosensing by Single-Molecule Encoded Nanoswitches. *Nano Lett.* **2020**, *20*, 2296.
(14) Use of a CDNA Microarray to Analyse Gene Expression Patterns in Human Cancer. *Nat. Genet.* **1996**, *14*, 457 DOI: 10.1038/ng1296-457.
(15) Abudayyeh, O. O.; Gootenberg, J. S.; Essletzbichler, P.; Han, S.; Joung, J.; Belanto, J. J.; Verdine, V.; Cox, D. B. T.; Kellner, M. J.; Regev, A.; Lander, E. S.; Voytas, D. F.; Ting, A. Y.; Zhang, F. RNA Targeting with CRISPR-Cas13. *Nature* **2017**, *550*, 280.
(16) He, X.; Wang, G.; Xu, G.; Zhu, Y.; Chen, L.; Zhang, X. A Simple, Fast, and Sensitive Assay for the Detection of DNA, Thrombin, and Adenosine Triphosphate Based on Dual-Hairpin DNA Structure. *Langmuir* **2013**, *29* (46), 14328−14334.
(17) Kékedy-Nagy, L.; Shipovskov, S.; Ferapontova, E. E. Effect of a Dual Charge on the DNA-Conjugated Redox Probe on DNA Sensing by Short Hairpin Beacons Tethered to Gold Electrodes. *Anal. Chem.* **2016**, *88* (16), 7984−7990.
(18) Su, S.; Ma, J.; Xu, Y.; Pan, H.; Zhu, D.; Chao, J.; Weng, L.; Wang, L. Electrochemical Analysis of Target-Induced Hairpin-Mediated Aptamer Sensors. *ACS Appl. Mater. Interfaces* **2020**, *12* (42), 48133−48139.
(19) Ling, P.; Lei, J.; Zhang, L.; Ju, H. Porphyrin-Encapsulated Metal−Organic Frameworks as Mimetic Catalysts for Electrochemical DNA Sensing via Allosteric Switch of Hairpin DNA. *Anal. Chem.* **2015**, *87* (7), 3957−3963.
(20) Farjami, E.; Clima, L.; Gothelf, K.; Ferapontova, E. E. Off−On" Electrochemical Hairpin-DNA-Based Genosensor for Cancer Diagnostics. *Anal. Chem.* **2011**, *83* (5), 1594−1602.
(21) Chen, J. I. L.; Chen, Y.; Ginger, D. S. Plasmonic Nanoparticle Dimers for Optical Sensing of DNA in Complex Media. *J. Am. Chem. Soc.* **2010**, *132* (28), 9600−9601.
(22) Chen, J. I. L.; Chen, Y.; Ginger, D. S. Plasmonic Nanoparticle Dimers for Optical Sensing of DNA in Complex Media. *J. Am. Chem. Soc.* **2010**, *132* (28), 9600−9601.
(23) Kovari, D. T.; Yan, Y.; Finzi, L.; Dunlap, D. Tethered Particle Motion: An Easy Technique for Probing DNA Topology and Interactions with Transcription Factors. *Methods Mol. Biol.* **2018**, *1665*, 317−340.
(24) Brinkers, S.; Dietrich, H. R. C.; De Groote, F. H.; Young, I. T.; Rieger, B. The Persistence Length of Double Stranded DNA Determined Using Dark Field Tethered Particle Motion. *J. Chem. Phys.* **2009**, *130* (21), 215105.
(25) Vanzi, F.; Sacconi, L.; Pavone, F. S. Analysis of Kinetics in Noisy Systems: Application to Single Molecule Tethered Particle Motion. *Biophys. J.* **2007**, *93* (1), 21−36.
(26) Pouget, N.; Turlan, C.; Destainville, N.; Salomé, L.; Chandler, M. IS911 Transpososome Assembly as Analysed by Tethered Particle Motion. *Nucleic Acids Res.* **2006**, *34* (16), 4313−4323.
(27) Schafer, D. A.; Gelles, J.; Sheetz, M. P.; Landick, R. Transcription by Single Molecules of RNA Polymerase Observed by Light Microscopy. *Nature* **1991**, *352* (6334), 444−448.
(28) Vanzi, F.; Broggio, C.; Sacconi, L.; Pavone, F. S. Lac Repressor Hinge Flexibility and DNA Looping: Single Molecule Kinetics by Tethered Particle Motion. *Nucleic Acids Res.* **2006**, *34* (12), 3409−3420.
(29) Mouliere, F.; Robert, B.; Peyrotte, E. A.; Del Rio, M.; Ychou, M.; Molina, F.; Gongora, C.; Thierry, A. R. High Fragmentation Characterizes Tumour-Derived Circulating DNA. *PLoS One* **2011**, *6*, No. e23418.
(30) Underhill, H. R.; Kitzman, J. O.; Hellwig, S.; Welker, N. C.; Daza, R.; Baker, D. N.; Gligorich, K. M.; Rostomily, R. C.; Bronner, M. P.; Shendure, J. Fragment Length of Circulating Tumor DNA. *PLoS Genet.* **2016**, *12* (7), No. e1006162.
(31) Braslavsky, I.; Amit, R.; Jaffar Ali, B. M.; Gileadi, O.; Oppenheim, A.; Stavans, J. Objective-Type Dark-Field Illumination for Scattering from Microbeads. *Appl. Opt.* **2001**, *40* (31), 5650.
(32) May, P. F. J.; Pinkney, J. N. M.; Zawadzki, P.; Evans, G. W.; Sherratt, D. J.; Kapanidis, A. N. Tethered Fluorophore Motion: Studying Large DNA Conformational Changes by Single-Fluorophore Imaging. *Biophys. J.* **2014**, *107* (5), 1205−1216.
(33) Sarfraz, N.; Khan, I. Plasmonic Gold Nanoparticles (AuNPs): Properties, Synthesis and Their Advanced Energy, Environmental and Biomedical Applications. *Chem. - Asian J.* **2021**, *16* (7), 720−742.
(34) Armstrong, R. E.; van Liempt, J. C.; Zijlstra, P. Effect of Film Thickness on the Far-and near-Field Optical Response of Nanoparticle-on-Film Systems Citation for Published Version (APA): Effect of Film Thickness on the Far-and Near-Field Optical Response of Nanoparticle-on-Film Systems. *J. Phys. Chem. C* **2019**, *123*, 25801.
(35) Mock, J. J.; Hill, R. T.; Tsai, Y.-J.; Chilkoti, A.; Smith, D. R. Probing Dynamically Tunable Localized Surface Plasmon Resonances of Film-Coupled Nanoparticles by Evanescent Wave Excitation. *Nano Lett.* **2012**, *12*, 1757.
(36) Visser, E. W. A.; Horáček, M.; Zijlstra, P. Plasmon Rulers as a Probe for Real-Time Microsecond Conformational Dynamics of Single Molecules. *Nano Lett.* **2018**, *18* (12), 7927−7934.
(37) Mock, J. J.; Hill, R. T.; Degiron, A.; Zauscher, S.; Chilkoti, A.; Smith, D. R. Distance-Dependent Plasmon Resonant Coupling between a Gold Nanoparticle and Gold Film. *Nano Lett.* **2008**, *8* (8), 2245−2252.
(38) Chen, T.; Hong, Y.; Reinhard, B. M. Probing DNA Stiffness through Optical Fluctuation Analysis of Plasmon Rulers. *Nano Lett.* **2015**, *15* (8), 5349−5357.
(39) Schwabl, F. Brownian Motion, Equations of Motion, and the Fokker−Planck Equations. In *Statistical Mechanics*; Schwabl, F., Ed.; Springer: Berlin, Heidelberg, 2006; pp 409−436, DOI: 10.1007/3-540-36217-7_8.
(40) Han, L.; Lui, B. H.; Blumberg, S.; Beausang, J. F.; Nelson, P. C.; Phillips, R. *Mathematics of DNA Structure, Function and Interactions*; Springer, 2009; Vol. *150*, DOI: 10.1007/978-1-4419-0670-0.
(41) Kumar, S.; Manzo, C.; Zurla, C.; Ucuncuoglu, S.; Finzi, L.; Dunlap, D. Enhanced Tethered-Particle Motion Analysis Reveals Viscous Effects. *Biophys. J.* **2014**, *106* (2), 399−409.
(42) Manghi, M.; Tardin, C.; Baglio, J.; Rousseau, P.; Salomé, L.; Destainville, N. Probing DNA Conformational Changes with High Temporal Resolution by Tethered Particle Motion. *Phys. Biol.* **2010**, *7* (4), No. 046003.
(43) van den Broek, B.; Vanzi, F.; Normanno, D.; Pavone, F. S.; Wuite, G. J. L. Real-Time Observation of DNA Looping Dynamics of Type IIE Restriction Enzymes NaeI and NarI. *Nucleic Acids Res.* **2006**, *34* (1), 167.
(44) Squires, T. M.; Messinger, R. J.; Manalis, S. R. Making It Stick: Convection, Reaction and Diffusion in Surface-Based Biosensors. *Nat. Biotechnol.* **2008**, *26*, 417−426.
(45) Gong, P.; Levicky, R. DNA Surface Hybridization Regimes. *Proc. Natl. Acad. Sci. U. S. A.* **2008**, *105* (14), 5301−5306.
(46) Tymoczko, J.; Schuhmann, W.; Gebala, M. Electrical Potential-Assisted DNA Hybridization. How to Mitigate Electrostatics for Surface DNA Hybridization. *ACS Appl. Mater. Interfaces* **2014**, *6*, 21851−21858.
(47) Sriram, M.; Markhali, B. P.; Nicovich, P. R.; Bennett, D. T.; Reece, P. J.; Brynn Hibbert, D.; Tilley, R. D.; Gaus, K.; Vivekchand, S. R. C.; Gooding, J. J. A Rapid Readout for Many Single Plasmonic Nanoparticles Using Dark-Field Microscopy and Digital Color Analysis. *Biosens. Bioelectron.* **2018**, *117*, 530−536.
(48) Verdoold, R.; Gill, R.; Ungureanu, F.; Molenaar, R.; Kooyman, R. P. H. Femtomolar DNA Detection by Parallel Colorimetric

Darkfield Microscopy of Functionalized Gold Nanoparticles. *Biosens. Bioelectron.* **2011**, *27* (1), 77−81.
(49) Duke, D. J.; Knast, T.; Edgington-Mitchell, D. Low Cost High Speed Digital Cameras for Experimental Fluid Mechanics. In *Proceedings of the 21st Australasian Fluid Mechanics Conference, AFMC 2018*; Australasian Fluid Mechanics Society, 2018.
(50) Visser, E. W. A.; van IJzendoorn, L. J.; Prins, M. W. J. Particle Motion Analysis Reveals Nanoscale Bond Characteristics and Enhances Dynamic Range for Biosensing. *ACS Nano* **2016**, *10*, 3093.
(51) Lubken, R. M.; De Jong, A. M.; Prins, M. W. J. How Reactivity Variability of Biofunctionalized Particles Is Determined by Superpositional Heterogeneities. *ACS Nano* **2021**, *15*, 1331.
(52) Murphy, M. C.; Rasnik, I.; Cheng, W.; Lohman, T. M.; Ha, T. Probing Single-Stranded DNA Conformational Flexibility Using Fluorescence Spectroscopy. *Biophys. J.* **2004**, *86* (4), 2530−2537.

https://doi.org/10.1021/acssensors.1c02097
ACS Sens. 2021, 6, 4297−4303